Acta Geologica Sinica (English Edition), 2022, 96(6): 2125–2134

First-principles Study on Equilibrium Sn Isotope Fractionations in Hydrothermal Fluids

SUN Mingguang[1, 2], Ryan MATHUR[3], CHEN Yanjing[2], YUAN Shunda[1] and WANG Jiaxin[1, *]

[1] *MNR Key Laboratory of Metallogeny and Mineral Assessment, Institute of Mineral Resources, Chinese Academy of Geological Sciences, Beijing 100037, China*
[2] *MOE Key Laboratory of Orogenic Belts and Crustal Evolution, Peking University, Beijing 100871, China*
[3] *Department of Geology, Juniata College, Huntingdon, PA 16652, USA*

Abstract: Tin (Sn) isotope geochemistry has great potential in tracing geological processes. However, lack of equilibrium Sn isotope fractionation factors of various Sn species limits the development of Sn isotope geochemistry. Equilibrium Sn isotope fractionation factors ($^{124}Sn/^{116}Sn$ and $^{122}Sn/^{116}Sn$) among various Sn(II, IV) complexes in aqueous solution were calculated using first-principles calculations. The results show that the oxidation states and the change of Sn(II, IV) species in hydrothermal fluids are the main factors leading to tin isotope fractionation in hydrothermal systems. For the Sn(IV) complexes, Sn isotope fractionation factors depend on the number of H_2O molecules. For the Sn(II) complexes, the Sn isotope fractionation between Sn(II)−F, Sn(II)−Cl and Sn(II)−OH complexes is mainly affected by the bond length and the coordination number of anion, whereas the difference in 1000lnβ values of Sn(II)−SO_4 and Sn(II)−CO_3 complexes is insignificant with the change of anion coordination number. By comparing the 1000lnβ values of all Sn(II, IV) complexes, the enrichment trend in heavy Sn isotopes is Sn(IV) complexes > Sn(II) complexes. The equilibrium Sn isotopic fractionation factors enhance our understanding of the tin transportation and enrichment processes in hydrothermal systems.

Key words: Sn isotope, isotope fractionation, first principles, tin species

Citation: Sun et al., 2022. First-principles Study on Equilibrium Sn Isotope Fractionations in Hydrothermal Fluids. Acta Geologica Sinica (English Edition), 96(6): 2125–2134. DOI: 10.1111/1755-6724.14923

1 Introduction

Tin (Sn) is a critical metal in the global high-tech industry. In recent years, metallogenesis and related mineral exploration of tin deposits has received increasing attention (Mao et al., 2019, 2021; Yuan et al., 2019; Yuan and Zhao, 2020). Previous studies have shown that 95% of the Sn resources in the world were extracted from tin deposits related to hydrothermal fluids (Lehmann, 1990, 2021). Therefore, investigating the transportation and enrichment processes of tin in hydrothermal fluids is crucial to better understanding the enrichment mechanism during tin mineralization. Many studies have shown that Sn(II) and Sn(IV) can combine with Cl^-, OH^-, F^-, SO_4^{2-} and CO_3^{2-} to form various complexes and they have identified a series of complex structures of tin in hydrothermal fluids (Jackson and Helgeson, 1985; Heinrich, 1990; Edwards et al, 1996; Sherman et al., 2000; Séby et al., 2001; Müller and Seward, 2001; Uchida et al., 2002; Cigala et al., 2012; Schmidt, 2018).

In recent years, with the rapid development of non-traditional isotope geochemistry, accurate determination of tin isotopic composition for geological samples has allowed us to use Sn isotope data to trace the process of tin mineralization (Badullovich et al., 2017; Mathur et al., 2017; Wang et al., 2019). The preliminary application of the Sn isotope in the study of hydrothermal tin mineralization shows that they can trace redox reactions that occurred during the formation of tin deposits (Brugger et al., 2016; Mason et al., 2016; Creech et al., 2017; Yao et al., 2018; She et al., 2020; Wang et al., 2021). Recent experiments by Wang et al. (2019) suggested that vaporation-induced fractionation results in the residual solution becoming isotopically lighter, and heavier Sn isotopes are favored in a stronger bonding environment associated with oxidation. The experimental study of Liu et al. (2021) shows that the Sn isotope can record the complex fluid evolution in a single cassiterite crystal. However, Sn(II) is easily oxidized at ambient conditions (Wang et al., 2019), and separating Sn(II) and Sn(IV) species in aqueous solution is difficult. This leads to the lack of equilibrium Sn isotope fractionation factors among the different Sn species, such as Sn−F, Sn−OH, Sn−CO_3, which has hampered the application of the Sn isotope in revealing the genesis of hydrothermal tin deposits.

With the rapid development of computational chemistry, the first-principles techniques have been widely used to calculate various isotope fractionations, especially for isotope systems that are difficult to determine the equilibrium fractionation factors under extreme experimental conditions (Schauble et al., 2003; Liu and

* Corresponding author. E-mail: jiaxin.wang@cags.ac.cn

http://www.geojournals.cn/dzxbcn/ch/index.aspx; https://onlinelibrary.wiley.com/journal/17556724

Tossell, 2005; Tossell, 2005; Li et al., 2009; Li and Liu, 2011; Huang et al., 2019; She et al., 2020; Gao and Liu, 2021; Wang, et al; 2021).

In this investigation, in order to comprehensively understand the equilibrium Sn isotope fractionation factors between various Sn complexes in hydrothermal solutions, we aimed to systematically calculate the fractionation between Sn(II, IV)−Cl, Sn(II)−OH, Sn(II)−F, Sn(II)−SO_4 and Sn(II)−CO_3 species using an implicit solvent model.

2 Methods

2.1 Reduced partition function ratio (β)

Here, we briefly summarize the definition of the terms and equations of the theories of equilibrium isotope fractionation (Chacko et al., 2001; Schauble, 2004; Liu et al., 2010; Dauphas and Schauble, 2016; Blanchard et al., 2017). Considering:

$$^{116}\mathrm{Sn}R + {}^{124}\mathrm{Sn} \leftrightharpoons {}^{124}\mathrm{Sn}R + {}^{116}\mathrm{Sn} \quad (1)$$

where R is a ligand of tin species. The reduced partition function ratios (βSnR or βSn) represent the fractionation factors between the interested phases and ideal gas atom of element Sn. The isotope fractionation factor (α) between two phases can be expressed as:

$$\alpha_{\mathrm{Sn}R-\mathrm{Sn}} = \beta_{\mathrm{Sn}R}/\beta_{\mathrm{Sn}} \quad (2)$$

in which, according to the Bigeleisen–Mayer equation (Bigeleisen and Mayer, 1947), the β factor is closely related to the vibrational frequencies of the corresponding phase:

$$\beta(\mathrm{A}) = \prod_i^N \frac{u_i^* \exp(-u_i^*/2)\left[1-\exp(-u_i)\right]}{u_i \exp(-u_i/2)\left[1-\exp(-u_i^*)\right]} \quad (3)$$

and

$$u_i = \frac{h\nu_i}{kT} \quad (4)$$

where N is the number of vibrational modes; ν_i is the harmonic vibrational frequency of its mode; h is Planck's constant; k is Boltzmann's constant and T is the temperature in Kelvin. Therefore, β only relates to the harmonic vibrational frequencies before and after the isotope substitution. If the vibrational frequencies of the isotope are known, the equilibrium isotope fractionations can be easily calculated. In this study, we report the reduced partition function ratio as 1000lnβ because it can easily be converted to 1000lnα_{A-B} by subtracting the β factors of the two complexes in equilibrium, Eq. (5):

$$1000\ln\alpha_{A-B} = 1000\cdot\ln\beta_A - 1000\cdot\ln\beta_B \quad (5)$$

2.2 Computational methods

We conducted the calculations using quantum chemical calculations with Gaussian 16; they were performed with three different basis sets: (1) the Becke-style3-parameter density function theory (B3LYP) with the Lee–Yang–Parr correlation functional (Lee et al., 1988; Becke, 1993a, b) with 6-311+G(d, p) basis sets for H, O, Cl, F and S and the Lan2DZ ECP pseudopotential for Sn; (2) B3LYP with 6-311+G(d, p) basis sets for H, O, Cl, F and S and SDD pseudopotential for Sn; and (3) B3LYP with def2-TZVP basis sets. After the vibrational frequencies were calculated, the reduced partition function ratios (β) were determined using Eq. 3. Through Eq. 5, the isotope fractionation factors are predicted.

2.3 Uncertainties of calculations of β factors by the implicit solvent model

The implicit solvent model (PCM method) defines the aqueous solution environment around the solute as a continuum of the uniform dielectric constant, which does not fully consider the dynamic characteristics of water and the interaction between water molecules (e.g., Liu and Tossell, 2005). To test whether our results are valid or not, we compared the calculated β values in the present work with those of previous theoretical study. Our calculation results show that the 1000ln$^{122/116}\beta$ values for $[Sn(IV)Cl_5(H_2O)]^-$ and $Sn(II)Cl_2$ calculated at the B3LYP/def2TZVP level at 25°C are 5.51‰ and 2.751‰, respectively, (Tables 3, 4), which are slightly lower than the values 5.29‰ and 2.62‰ calculated by Wang et al. (2021) using the explicit solvent model. The 1000lnα$[Sn(IV)Cl_5(H_2O)]^-$−$Sn(II)Cl_2$ values are 2.759‰ and 2.670‰, and the difference is 0.089‰.

3 Results

3.1 Geometric properties of Sn species in solution

In this study, three different theoretical levels were used to optimize the structures and then the harmonic vibration of all species was analyzed (Table 1); the bond lengths of these species are listed in Table 2. The Sn−O bond length of $[Sn(OH)_3]^-$ and the Sn−Cl bond length of $[Sn^{2+}Cl_3]^-$ measured by previous experiments were 2.078 Å and 2.47 Å, respectively (Table 2) (Chen and Grandbois, 2013; Bajnóczi et al., 2014), which are consistent with the calculate bond lengths (Table 2) by B3LYP/def2−TZVP (2.076 Å and 2.524 Å). The comparison between calculated values and experimental values shows that bond lengths calculated by the B3LYP/def2−TZVP method are accurate and reliable. Therefore, the harmonic vibration frequencies of all Sn complexes were calculated using the B3LYP/def2−TZVP method; the optimized molecular structures of these species are shown in Fig. 1 (Sn−OH species), Fig. 2 (Sn−F and Sn−Cl species) and Fig. 3 (Sn−CO_3 and Sn−SO_4 species).

The geometric properties of the Sn−OH, Sn−Cl and Sn−F complexes are shown in Table 2. The results show that the bond lengths of Sn(II)−Cl are significantly longer than those of Sn(II)−F and Sn(II)−OH, whereas the bond lengths of Sn(II)−F and Sn(II)−OH are almost equal (Table 4) at the same coordination number. The variation rule of bond length of Sn(II)−CO_3 and Sn(II)−SO_4 is not obvious. The geometric properties of Sn(IV) species are shown in Table 2 and Fig. 5. The average Sn−Cl bond lengths of $[Sn^{4+}Cl_4]^0$, $[Sn^{4+}Cl_3\cdot 3H_2O]^+$, $[Sn^{4+}Cl_4\cdot 2H_2O]^0$, $[Sn^{4+}Cl_5\cdot H_2O]^-$ and $[Sn^{4+}Cl_6]^{2-}$, are 2.32 Å, 2.36 Å, 2.41 Å, 2.44 Å and 2.49 Å, respectively, which increase gradually with the increase of the number of Cl atoms in the solute molecules.

Table 1 Calculations of the main tin(II, IV)-bearing complexes obtained by previous experiments

Sn(II, IV) species in solution			Reference
Sn(II) species	Sn(II)−OH species	$[Sn(OH)]^+$ $[Sn(OH)_2]^0$ $[Sn(OH)_3]^-$ $[Sn^{2+}OHCl]^0$	Jackson and Helgeson,1985; Dokic et al., 1991; Djurdjevic et al., 1995; Séby et al., 2001; Cigala et al., 2012
	Sn(II)−Cl species	$[Sn^{2+}Cl]^+$ $[Sn^{2+}Cl_2]$ $[Sn^{2+}Cl_3]^-$	Bond and Taylor, 1970; Pettine et al., 1981; Müller and Seward, 2001; Séby et al., 2001; Cigala et al., 2012; Wang et al., 2021
	Sn(II)−F species	$[Sn^{2+}F]^+$ $[Sn^{2+}F_2]^0$ $[Sn^{2+}F_3]^-$	
	Sn(II)−CO_3^{2-},SO_4^{2-} species	$[Sn^{2+}CO_3]^0$ $[Sn^{2+}HCO_3]^+$ $[Sn^{2+}(OH)CO_3]^-$ $[Sn^{2+}SO_4]^0$	Cigala et al., 2012
Sn(IV) species	Sn(IV)−Cl/H_2O species	$[Sn^{4+}Cl_4]$ $[Sn^{4+}Cl_6]^{2-}$ $[Sn^{4+}Cl_5{\cdot}H_2O]^-$ $[Sn^{4+}Cl_4{\cdot}2H_2O]$ $[Sn^{4+}Cl_3{\cdot}3H_2O]^+$	Sherman et al., 2000; Schmidt, 2018; She et al., 2020; Wang et al., 2021

Table 2 Comparison of bond lengths and experimental values of Sn(II, IV) complexes optimized at different theoretical and basis set levels

Speciation	Average bond length of Sn-X	Bond length (Å)		
		B3LYP/6-311G+(d, p)/Lan2DZ	B3LYP/6-311G+(d, p)/SDD	B3LYP/def2tzvp
$[Sn(OH)_3]^-$	Sn−O	2.03113	2.0969	2.0762
	Exp	2.078[a]		
$[Sn^{2+}OH]^+$	Sn−O	1.84026	1.8955	2.014
$[Sn^{2+}(OH)_2]^0$	Sn−O	1.95928	2.02512	2.063
$[Sn^{2+}Cl]^+$	Sn−Cl	2.42491	2.45457	2.44893
$[Sn^{2+}Cl_2]$	Sn−Cl	2.53041	2.55935	2.50838
$[Sn^{2+}Cl_3]^-$	Sn−Cl	2.61875	2.64729	2.52367
	Exp	2.475[a]		
$[Sn^{2+}F]^+$	Sn−F	1.89758	1.9578	1.98808
$[Sn^{2+}F_2]^0$	Sn−F	1.94954	2.00906	2.02325
$[Sn^{2+}F_3]^-$	Sn−F	1.99745	2.05801	2.02494
$[Sn^{4+}Cl_4]$	Sn−Cl	2.37704	2.40718	2.31749
$[Sn^{4+}Cl_3{\cdot}3H_2O]^+$	Sn−Cl	2.42669	2.45269	2.35531
$[Sn^{4+}Cl_4{\cdot}2H_2O]$	Sn−Cl	2.46868	2.49477	2.40554
$[Sn^{4+}Cl_5{\cdot}H_2O]^-$	Sn−Cl	2.48360	2.52729	2.43911
$[Sn^{4+}Cl_6]^{2-}$	Sn−Cl	2.53319	2.56321	2.48571
				Raman spectra
$[Sn^{2+}Cl_2]$	Calculated value			273
	Exp			272[b]

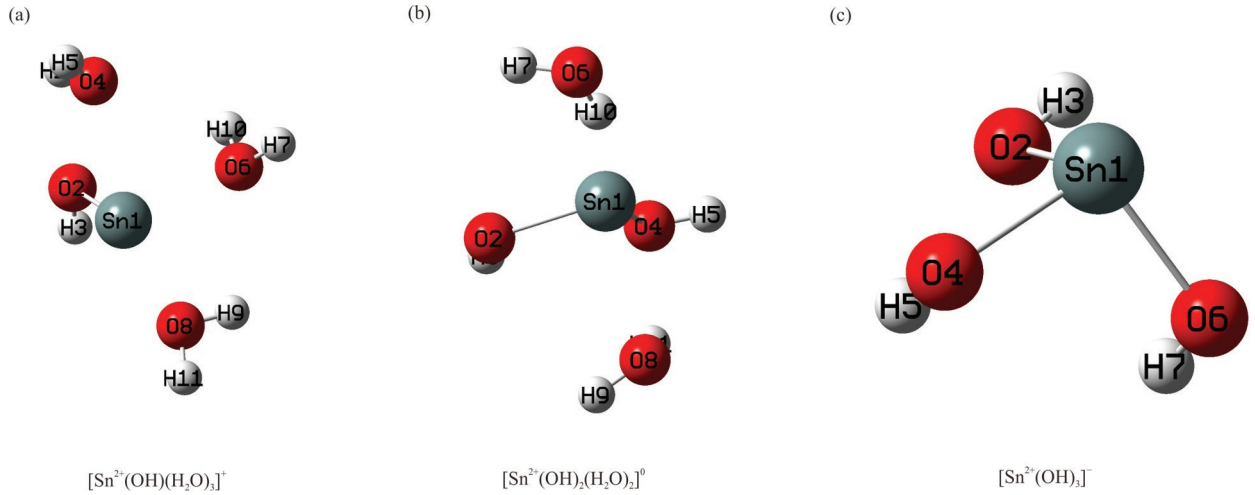

Fig. 1. Molecular structure of Sn(II)−OH species in aqueous solution.
(a) $[Sn^{2+}(OH)(H_2O)_3]^+$; (b) $[Sn^{2+}(OH)_2(H_2O)_2]^0$; (c) $[Sn^{2+}(OH)_3(H_2O)]^-$.

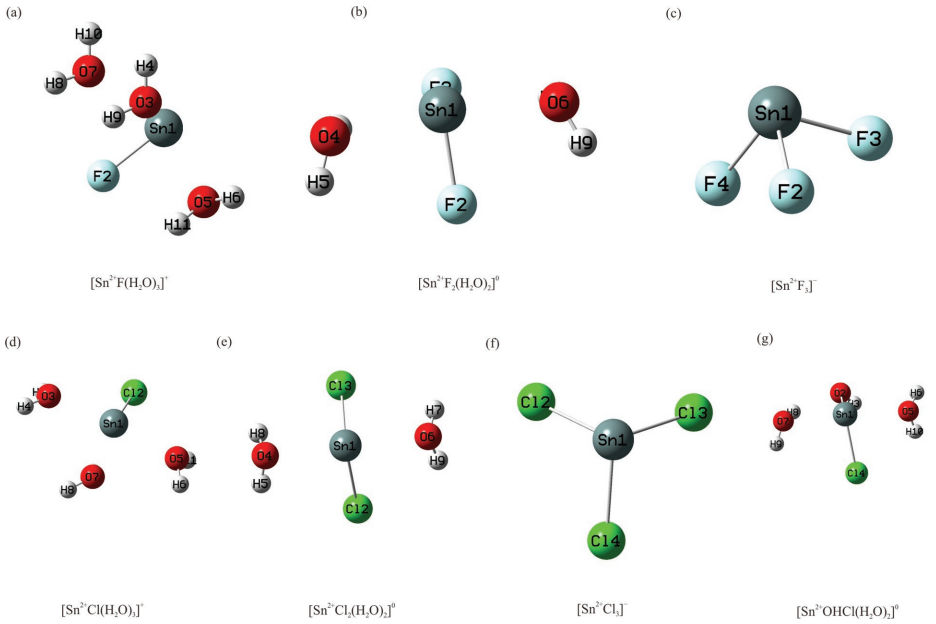

Fig. 2. Molecular structure of Sn(II)−F and Sn(II)−Cl species in aqueous solution.
(a) $[Sn^{2+}F(H_2O)_3]^+$; (b) $[Sn^{2+}F_2(H_2O)_2]^0$; (c) $[Sn^{2+}F_3(H_2O)]^-$; (d) $[Sn^{2+}Cl(H_2O)_3]^+$; (e) $[Sn^{2+}Cl_2(H_2O)_2]^0$; (f) $[Sn^{2+}Cl_3(H_2O)]^-$; (g) $[Sn^{2+}OHCl(H_2O)_2]^0$.

3.2 β values of Sn-bearing aqueous species

We systematically calculated the $1000\ln^{124/116}\beta$ and $1000\ln^{122/116}\beta$ values of all Sn complexes at different temperatures, as shown in Tables 3 and 4. The $1000\ln\beta$ values decreased with an increase in temperature, and the $1000\ln^{124/116}\beta$ value of the same complex is greater than the $1000\ln^{122/116}\beta$ value (Tables 3, 4) at constant temperature. Here, we calculated the equilibrium Sn isotope fractionation factors of Sn−OH species, Sn−CO_3, Sn−SO_4 and Sn−F species for the first time and the $1000\ln^{124/116}\beta$ ($1000\ln^{122/116}\beta$) values of these species at different temperature are listed in Table 3.

In order to investigate the Sn isotope fractionation between Sn(II)−F species, Sn(II)−OH species and Sn(II)−Cl species, we used the implicit solvent model to calculate the $1000\ln^{124/116}\beta$ ($1000\ln^{122/116}\beta$) values of Sn(II)−Cl species that were calculated by explicit solvent model (Wang et al., 2021). The results show that the β factors of the Sn–Cl species are smaller than those of Sn(II)−F and Sn(II)−OH, whereas the difference in the equilibrium Sn isotope fractionation factors between Sn(II)−F and Sn(II)−OH species is small at the same coordination number. For the Sn(IV) complexes, the $1000\ln^{124/116}\beta$ ($1000\ln^{122/116}\beta$) values of $[Sn^{4+}Cl_4]^0$, $[Sn^{4+}Cl_3{\cdot}3H_2O]^+$, $[Sn^{4+}Cl_4{\cdot}2H_2O]^0$, $[Sn^{4+}Cl_5{\cdot}H_2O]^-$ and $[Sn^{4+}Cl_6]^{2-}$ are listed in Table 4, and the $1000\ln\beta$ values decreased gradually with the increase in the number of Cl atoms in the solute molecules. In general, the β factors of the Sn(IV) complex is larger than that of the Sn(II) complex.

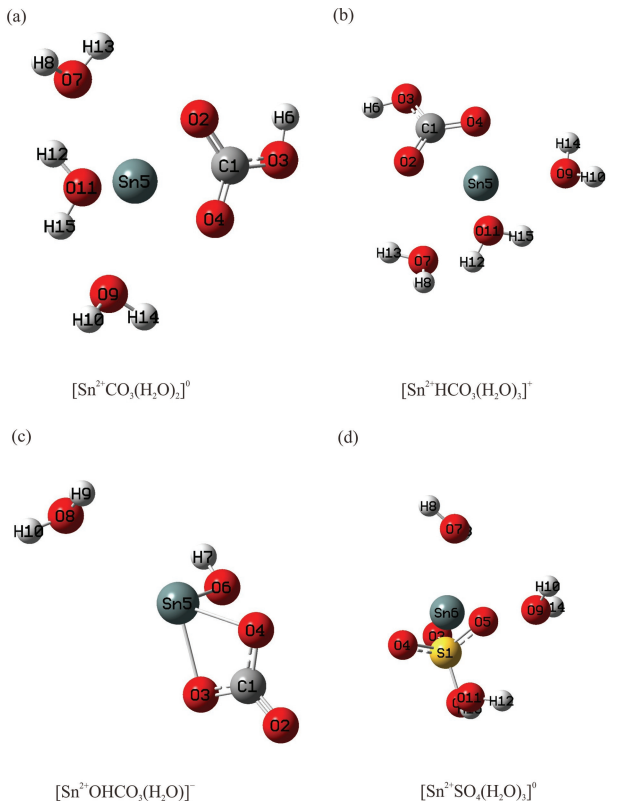

Fig. 3. Molecular structure of Sn(II)−CO_3^{2-} and Sn(II)−SO_4^{2-} species in aqueous solution.
(a) $[Sn^{2+}CO_3(H_2O)_2]^0$; (b) $[Sn^{2+}HCO_3(H_2O)_3]^+$; (c) $[Sn^{2+}OHCO_3(H_2O)]^-$; (d) $[Sn^{2+}SO_4(H_2O)_3]^0$.

4 Discussion

4.1 Isotope fractionation between various complexes of Sn(II)

4.1.1 Isotope fractionation between Sn(II)−OH complexes

Previous studies have demonstrated that the hydrolysis of tin (II) in aqueous solutions widely occur at pH ≥ 2, and the three products of the hydrolysis, namely: [Sn(II)

Table 3 Values of 1000ln$^{124/116}\beta$ and 1000ln$^{122/116}\beta$ of Sn(II) species (25°C −300°C)

Speciation	1000ln$^{124/116}\beta$				1000ln$^{122/116}\beta$			
	25°C	100°C	200°C	300°C	25°C	100°C	200°C	300°C
$[Sn^{2+}OH]^+$	3.82	2.506	1.589	1.095	2.924	1.919	1.217	0.838
$[Sn^{2+}(OH)_2]^0$	4.558	3.003	1.91	1.318	3.491	2.299	1.462	1.009
$[Sn^{2+}(OH)_3]^-$	5.7095	3.7423	2.3714	1.633	4.355	2.855	1.809	1.246
$[Sn^{2+}Cl]^+$	2.79	1.805	1.135	0.778	2.156	1.395	0.877	0.602
$[Sn^{2+}Cl_2]$	2.751	1.774	1.111	0.76	2.092	1.349	0.845	0.578
$[Sn^{2+}Cl_3]^-$	2.8959	1.8620	1.1637	0.7951	2.2167	1.4253	0.8908	0.6086
$[Sn^{2+}OHCl]$	3.647	2.384	1.508	1.037	2.793	1.825	1.155	0.794
$[Sn^{2+}F]^+$	3.868	2.522	1.589	1.089	2.945	1.918	1.208	0.827
$[Sn^{2+}F_2]^0$	4.785	3.134	1.985	1.367	3.672	2.406	1.525	1.05
$[Sn^{2+}F_3]^-$	5.8553	3.82527	2.4175	1.6618	4.4777	2.925	1.848	1.271
$[Sn^{2+}CO_3]$	3.895	2.535	1.599	1.099	2.985	1.942	1.225	0.842
$[Sn^{2+}HCO_3]^+$	2.683	1.711	1.056	0.713	1.967	1.247	0.765	0.513
$[Sn^{2+}(OH)CO_3]^-$	5.26	3.436	2.173	1.495	4.018	2.625	1.66	1.142
$[Sn^{2+}SO_4]^0$	3.454	2.214	1.369	0.922	2.742	1.752	1.079	0.724

Table 4 Values of 1000ln $^{124/116}\beta$ and 1000ln$^{122/116}\beta$ of Sn(IV) complexes (25°C–300°C)

Speciation	1000ln $^{124/116}\beta$				1000ln$^{122/116}\beta$			
	25°C	100°C	200°C	300°C	25°C	100°C	200°C	300°C
$[Sn^{4+}Cl_4]$	7.57	4.91	3.09	2.12	5.80	3.77	2.37	1.62
$[Sn^{4+}Cl_3{\cdot}3H_2O]^+$	7.30	4.74	2.98	2.05	5.58	3.62	2.28	1.57
$[Sn^{4+}Cl_4{\cdot}2H_2O]$	6.63	4.29	2.69	1.84	5.05	3.27	2.05	1.40
$[Sn^{4+}Cl_5{\cdot}H_2O]^-$	5.51	3.55	2.23	1.52	4.59	2.97	1.86	1.27
$[Sn^{4+}Cl_6]^{2-}$	5.27	3.39	2.12	1.45	4.04	2.60	1.62	1.11

$(OH)]^+$, $[Sn(II)(OH)_2]^0$ and $[Sn(II)(OH)_3]^-$, have been identified by experiments (Djurdjevic et al., 1995; Séby et al., 2001; Cigala et al., 2012). Here, we have calculated the values of 1000ln$^{124/116}\beta$ and 1000ln$^{122/116}\beta$ for Sn(II)−OH species at 25, 100, 200 and 300°C (Table 3). The 1000ln$^{124/116}\beta$ values of $[Sn^{2+}OH(H_2O)_3]^+$, $[Sn^{2+}(OH)_2(H_2O)_2]^0$ and $[Sn^{2+}(OH)_3]^-$ are 3.820‰, 4.558‰ and 6.046‰, respectively, at 25°C.The average Sn−O bond lengths of $[Sn^{2+}OH(H_2O)_3]^+$, $[Sn^{2+}(OH)_2(H_2O)_2]^0$ and $[Sn^{2+}(OH)_3]^-$ are 2.014 Å, 2.0633 Å and 2.0762 Å, respectively. The data show that one, two and three Sn−O bonds are formed in $[Sn^{2+}OH(H_2O)_3]^+$, $[Sn^{2+}(OH)_2(H_2O)_2]^0$ and $[Sn^{2+}(OH)_3]^-$ (Fig. 1), respectively. Though bond length increases and bond strength weakens with the increase in the number of OH, the greater the amount of OH^-, the stronger the bond environment provided to tin (Table 2, 3). Therefore, the 1000lnβ values of Sn−OH species increases with the increase of the amount of OH^-, indicating that the influence of bonding environment on the 1000lnβ value is stronger than bond length. This leads to the enrichment order of the heavy isotope of Sn (II) in solution is $[Sn(II)(OH)_3]^- > [Sn(II)(OH)_2(H_2O)_2]^0 > [Sn(II)(OH)(H_2O)_3]^+$ at constant temperature (Fig. 4).

4.1.2 Isotope fractionation between Sn(II)−F and Sn(II)−Cl complexes

A large number of studies have shown that fluorine and chlorine are ubiquitous components in the granitic magmatic−hydrothermal tin mineralization, indicating that Cl and F probably play important roles for tin transportation in hydrothermal fluids (Helgeson, 1969; Bailey, 1977; White et al., 1981; Zhu and Sverjensky, 1992). Field observations have also shown that the fluorite intergrowth with cassiterite is ubiquitous in tin ore (Wang et al., 2012; Mohamed, 2013; Guo et al., 2018). In addition, previous experimental studies suggested that the solubility of Sn(II) in HF-bearing and HCl-bearing fluids are 70−2000 ppm (0.5−3.2 m HF) and 0.8 to 11 wt% (0.5−4.4 m HCl) at 700°C, 140 MPa (Duc-Tin et al., 2007), respectively, which indicate that Sn maybe transported as Sn(II)−F and Sn(II)−Cl complexes in ore-forming fluids. Previous experimental studies of potentiometry, solubility, spectrophotometry, polarography and new voltametric measurements on tin in hydrothermal fluids have suggested that the Sn(II) complexes combined with F and Cl in solution mainly include $[Sn(II)F(H_2O)_3]^+$, $[Sn(II)F_2(H_2O)_2]^0$, $[Sn(II)F_3]^-$, $[Sn(II)Cl(H_2O)_3]^+$, $[Sn(II)Cl_2(H_2O)_2]$, $[Sn(II)Cl_3]^-$ and $[Sn(II)OHCl(H_2O)_2]^0$ (i.e., Müller and Seward, 2001; Séby et al., 2001; Cigala et al., 2012).

Here, we calculated the Sn isotope fractionation of between different Sn(II)−F species and Sn(II)−Cl species. The 1000ln$^{124/116}\beta$ and 1000ln$^{122/116}\beta$ values of Sn(II)−F and Sn(II)−Cl species at 25, 100, 200 and 300°C (Table 3) show that the heavy Sn isotope enrichment order of tin in the solution is $[Sn(II)F_3]^- > [Sn(II)F_2(H_2O)_2]^0 > [Sn(II)F(H_2O)_3]^+ > [Sn(II)OHCl(H_2O)_2]^0 > [Sn(II)Cl_3]^- > [Sn(II)Cl(H_2O)_3]^+ > [Sn(II)Cl_2(H_2O)_2]$ at constant temperature (Fig. 4). The calculated results show that the bond length of Sn (II)−Cl is significantly longer than that of Sn(II)−OH and Sn(II)−F (Table 2), which led to the enrichment of light isotopes in Sn(II)−Cl complexes and the enrichment of heavy isotopes in Sn(II)−OH and Sn(II)−F complexes. This is consistent with that shorter bonds are stronger, and more favorable to the heavy isotopes relative to the longer bonds (Urey, 1947; Schauble, 2004; Young et al., 2009; Huang et al., 2013, 2014).

4.1.3 Isotope fractionation between Sn(II)−CO_3 and Sn (II)−SO_4 complexes

Some skarn cassiterite−sulfide deposits are accompanied by carbonate alteration, such as Mount Biscoff, Cleveland deposits in Australia (Collins, 1981; Halley and Walshe, 1995), and the experimental studies showed that SnO_2 has high solubility in the alkali carbonate aqueous solution during heating (Liu et al, 2020). Moreover, the studies of Eadington (1983) and Barsukov and Suschevskaya (1973) have shown that the importance of SO_4^{2-} relative to Cl^- ions is increasing in later lower temperature and HCO_3^- could be dominant

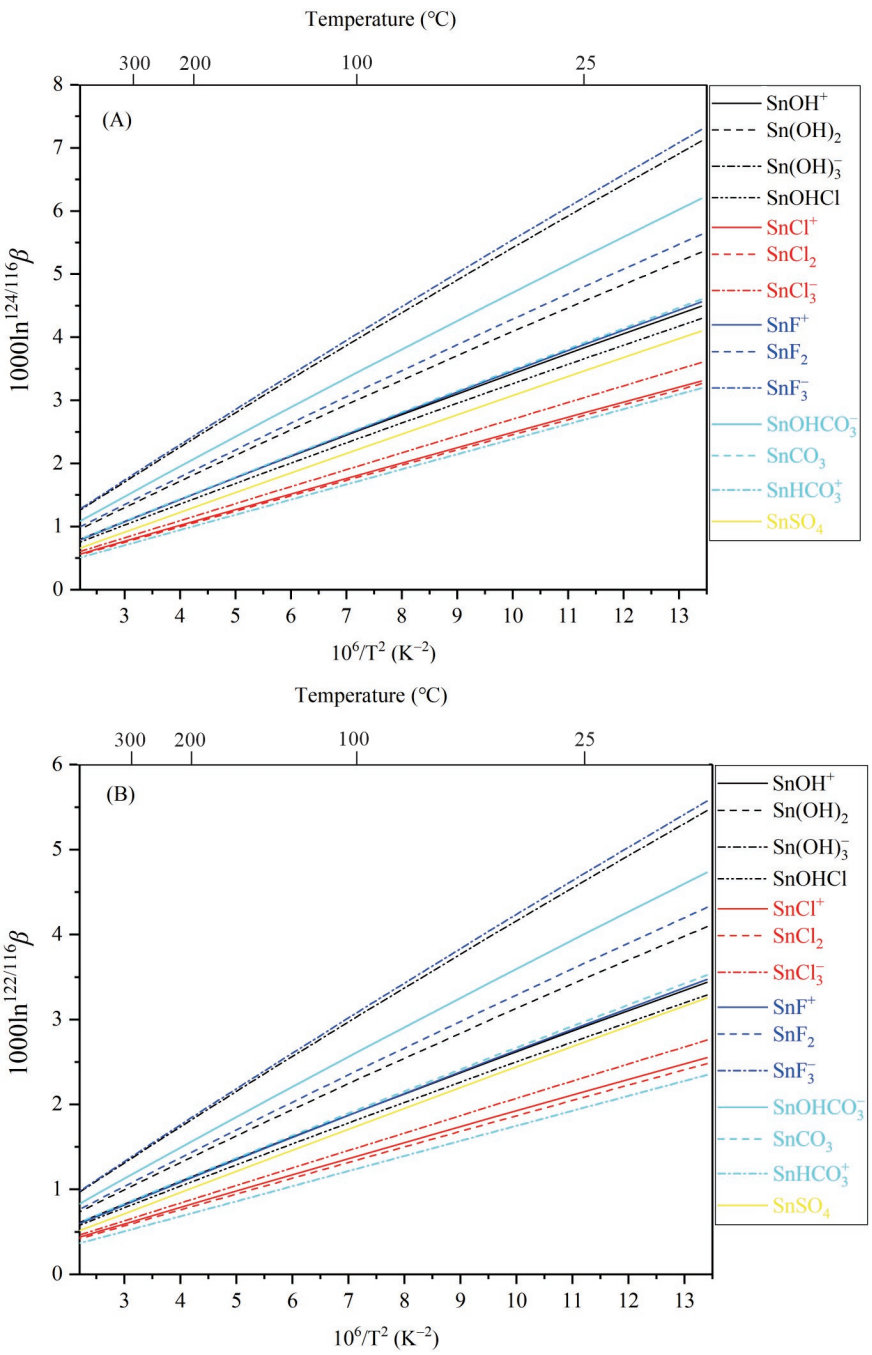

Fig. 4. Calculated 1000ln$^{124/116}\beta$ (A) and 1000ln$^{122/116}\beta$ (B) values for Sn(II) species in aqueous solution.

or significant anion in fluids associated with many tin deposits. This suggested that Sn(II) can also be probably transported as Sn(II)−CO_3^{2-} or Sn(II)−SO_4^{2-} complexes in ore-forming fluids. Up to now, there are four Sn(II) species combined with CO_3^{2-} and SO_4^{2-} in hydrothermal fluid have been identified by experiments (Cigala et al., 2012), including $[Sn(II)CO_3]^0$, $[Sn(II)HCO_3]^+$, $[Sn(II)(OH)CO_3]^-$ and $[Sn(II)SO_4]^0$. In this study, we calculated the values of 1000lnβ for those Sn(II) species at different temperature, and the results are present in Table 3.

The 1000lnβ values of $[Sn(II)(OH)CO_3]^-$, $[Sn(II)CO_3]^0$, $[Sn(II)HCO_3]^+$ and $[Sn(II)SO_4]^0$ are 5.260‰, 3.895‰, 2.683‰ and 3.454‰, respectively, and complexes containing OH ligands are higher than those of complexes without OH^- ligands (Table 3; Fig. 4), which determines that the heavy Sn isotope enrichment order was $[Sn(II)(OH)CO_3]^- > [Sn(II)CO_3]^0 > [Sn(II)SO_4]^0 > [Sn(II)HCO_3]^+$ (Fig. 4).

4.2 Isotope fractionation between Sn(IV) complexes

Although most of the previous studies suggest that tin mainly transport as Sn(II) species in the magmatic−hydrothermal process (i.e., Sherman et al.,

2000; Duc-Tin et al., 2007), some recent studies show that Sn(IV) complexes can also be transported in the hydrothermal fluids (Schmidt, 2018; Wang et al., 2021), and the Sn(IV) complexes in the solution mainly include $[Sn(IV)Cl_3{\cdot}3H_2O]^+$, $[Sn(IV)Cl_4{\cdot}2H_2O]$, $[Sn(IV)Cl_4]$, $[Sn(IV)Cl_5{\cdot}H_2O]^-$ and $[Sn(IV)Cl_6]^{2-}$ (Sherman et al., 2000; Schmidt, 2018). Here, we optimized the molecular structures and calculated harmonic frequencies of various Sn(IV) species (Fig. 5). By comparing the $1000\ln^{124/116}_{(122/116)}\beta$ values and Sn−Cl bond length of those Sn(IV) species (Table 2), it is suggested that as the H_2O molecules in Sn−Cl−H_2O complexes are gradually replaced by Cl ions, Sn−Cl bond length of those species increase gradually, 2.36 Å, 2.41 Å, 2.44 Å and 2.49 Å, the $1000\ln\beta$ values of those complexes decrease gradually at constant temperature (Table 4). This leads to a enrichment trend of heavy tin isotope as: $[Sn(IV)Cl_4]$ > $[Sn(IV)Cl_3{\cdot}3H_2O]^+$ > $[Sn(IV)Cl_4{\cdot}2H_2O]$ > $[Sn(IV)Cl_5{\cdot}H_2O]^-$ > $[Sn(IV)Cl_6]^{2-}$ (Table 4), which is consistent with the enrichment trend of Sn isotope fractionation calculated by She et al. (2020).

4.3 Tin isotope fractionation caused by valence change between Sn(II) and Sn(IV) in aqueous solution

In the process of transport and enrichment of tin in magmatic hydrothermal fluid, the change of redox condition is an important controlling factor of tin mineralization (Heinrich, 1990), and the Sn isotope investigation suggested that the variation of valance state is the main factor controlling the Sn isotope fractionation (Yao et al., 2018). In addition, Roskosz et al. (2020) also concluded that large tin isotope fractionation is expected between materials containing Sn^{2+} and Sn^{4+}. Here, we calculated the $1000\ln\beta$ values of Sn(IV)−Cl species and Sn(II)−Cl species in solution. The results show that the $^{124/116}$Sn fractionations between Sn(IV) and Sn(II) complexes is up to 4.88 ‰ ($1000\ln\alpha_{SnCl_4-SnHCO_3^-}$) at 25°C, which indicate that the valence state change of Sn in aqueous solution leads to significant Sn isotope fractionation. Our calculation results are consistent with the conclusions of Yao et al. (2018) and Roskosz et al. (2020).

In addition, we also calculated the Sn isotope fractionation between Sn(II)−OH, Sn(II)−F, Sn(II)−SO_4, Sn(II)−CO_3 species and Sn(IV)−Cl species. Among these complexes (Table 1), the variation of valence state leads to large Sn isotopic fractionation at 25°C ($1000\ln\alpha_{Sn(IV)-Sn(II)}$ = 1.411‰–5.772‰). However, the difference of $1000\ln\beta$ values between these complexes ($[Sn(II)F_3]^-$, $[Sn(II)(OH)_3]^-$, $[Sn(II)(OH)CO_3]^-$, $[Sn(IV)Cl_6]^{2-}$ and $[Sn(IV)Cl_5{\cdot}H_2O]^-$) is very small, and the Sn isotope fractionation caused by the valence change is also small at constant temperature (Table 5). Our calculation results suggest that the total enrichment trend of heavy Sn

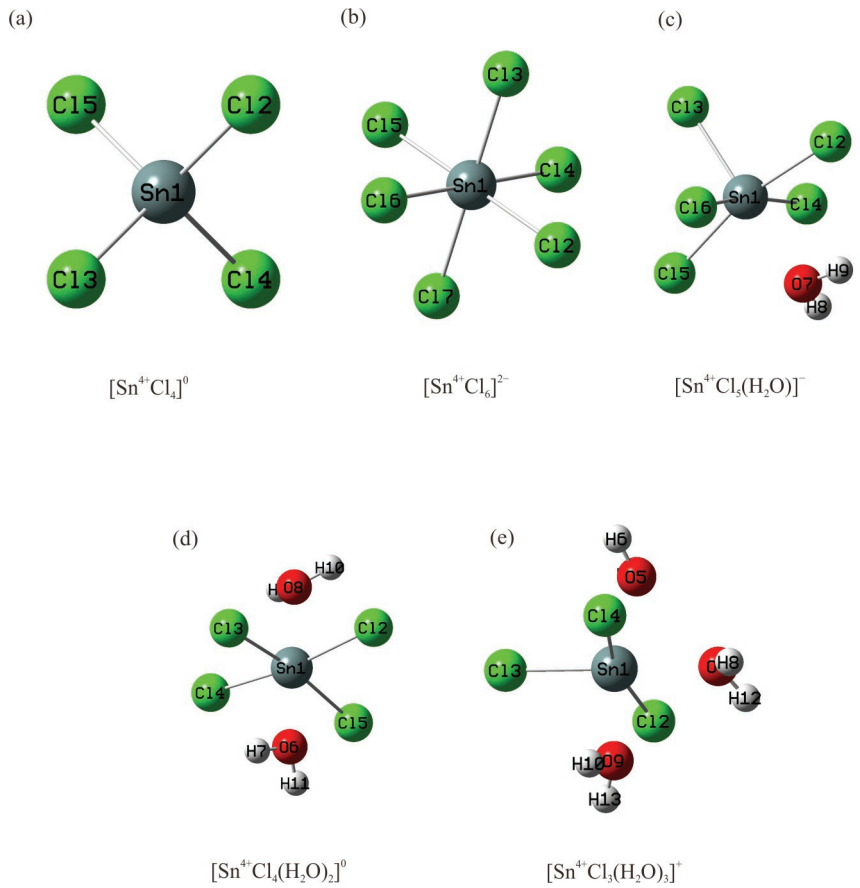

Fig. 5. Species of Sn(IV) in aqueous solution.
(a) $[Sn^{4+}Cl_4]$; (b) $[Sn^{4+}Cl_6]^{2-}$; (c) $[Sn^{4+}Cl_5(H_2O)]^-$; (d) $[Sn^{4+}Cl_4(H_2O)_2]$; (e) $[Sn^{4+}Cl_3(H_2O)_3]^+$.

Table 5 1000ln$\alpha^{124/116}Sn_{A-B}$ values between any two Sn(II, IV)-bearing aqueous species at 25°C

	a	b	c	d	e	f	g	h	i	j	k	l	m	n	o	p	q	r	s
a	0.00	−0.92	−2.32	1.08	1.12	0.84	0.41	−0.69	−0.03	−1.39	0.22	−2.18	1.19	0.05	−3.43	−3.70	−2.76	−1.64	−1.40
b		0.00	−1.41	1.99	2.03	1.75	1.33	0.23	0.89	−0.48	1.14	−1.26	2.10	0.96	−2.51	−2.78	−1.84	−0.72	−0.49
c			0.00	3.40	3.44	3.16	2.74	1.63	2.30	0.93	2.55	0.15	3.51	2.37	−1.10	−1.38	−0.44	0.68	0.92
d				0.00	0.04	−0.24	−0.66	−1.77	−1.10	−2.47	−0.86	−3.26	0.11	−1.03	−4.51	−4.78	−3.84	−2.72	−2.48
e					0.00	−0.28	−0.70	−1.81	−1.14	−2.51	−0.90	−3.29	0.07	−1.07	−4.54	−4.82	−3.88	−2.76	−2.52
f						0.00	−0.42	−1.53	−0.86	−2.23	−0.61	−3.01	0.35	−0.79	−4.26	−4.54	−3.60	−2.48	−2.24
g							0.00	−1.10	−0.44	−1.81	−0.19	−2.59	0.77	−0.37	−3.84	−4.11	−3.17	−2.05	−1.82
h								0.00	0.66	−0.70	0.91	−1.49	1.88	0.74	−2.74	−3.01	−2.07	−0.95	−0.71
i									0.00	−1.36	0.25	−2.15	1.21	0.08	−3.40	−3.67	−2.73	−1.61	−1.38
j										0.00	1.61	−0.79	2.58	1.44	−2.04	−2.31	−1.37	−0.25	−0.01
k											0.00	−2.40	0.96	−0.17	−3.65	−3.92	−2.98	−1.86	−1.62
l												0.00	3.36	2.23	−1.25	−1.52	−0.58	0.54	0.77
m													0.00	−1.14	−4.61	−4.88	−3.94	−2.82	−2.59
n														0.00	−3.48	−3.75	−2.81	−1.69	−1.45
o															0.00	−0.27	0.67	1.79	2.03
p																0.00	0.94	2.06	2.30
q																	0.00	1.12	1.36
r																		0.00	0.24
s																			0.00

Note: a. $[Sn^{2+}F]^{+}$, b.$[Sn^{2+}F_2]^{0}$, c. $[Sn^{2+}F_3]^{-}$, d. $[Sn^{2+}Cl]^{+}$, e. $[Sn^{2+}Cl_2]$, f. $[Sn^{2+}Cl_3]^{-}$, g. $[Sn^{2+}SO_4]^{0}$, h. $[Sn^{2+}(OH)_2]^{0}$, i. $[Sn^{2+}CO_3]$, j. $[Sn^{2+}(OH)CO_3]^{-}$, k. $[Sn^{2+}OHCl]^{0}$, l. $[Sn^{2+}(OH)_3]^{-}$, m. $[Sn^{2+}HCO_3]^{+}$, n. $[Sn^{2+}OH]^{+}$, o. $[Sn^{4+}Cl_3{\cdot}3H_2O]^{+}$, p. $[Sn^{4+}Cl_4]$, q. $[Sn^{4+}Cl_4{\cdot}2H_2O]$, r. $[Sn^{4+}Cl_5{\cdot}H_2O]^{-}$, s. $[Sn^{4+}Cl_6]^{2-}$.

isotope is Sn(IV) species > Sn(II) species (Tables 3 and 4). In fact, the enrichment trend of Sn isotope in magma is the same as that in hydrothermal fluids (Badullovich et al., 2017; Creech et al., 2017; Wang et al., 2018; Roskosz et al., 2020).

5 Conclusions

In this study, we systematically calculated the fractionation between Sn(II, IV)−Cl, Sn(II)−OH, Sn(II)−F, Sn(II)−SO_4 and Sn(II)−CO_3 species using an implicit solvent model.

We estimate that the equilibrium Sn isotope fractionation factors between several important processes leads to transportation, and enrichment of tin. Our calculations predict significant Sn isotope fractionation among Sn species with different valences, following a general trend of enrichment of ^{124}Sn (^{122}Sn) as Sn(IV) species > Sn(II) species.

The main factors leading to tin isotope fractionation are as follows: (1) isotope fractionation between Sn(II) species in hydrothermal fluids is mainly affected by the speciation and bond length, and Sn(II)−Cl species will enrich light Sn isotopes relative to the Sn(II)−OH and Sn (II)−F species; and (2) isotope fractionation between Sn (IV) species in hydrothermal fluids is affected by the coordination number of ligands (Cl^- and H_2O). These basic equilibrium Sn isotope fractionation factors provided in this study will allow us to further study the transportation, and enrichment mechanism of tin in hydrothermal systems by Sn isotope tracer.

Acknowledgments

We sincerely thank the reviewers for their constructive comments on this article, which have greatly improved it. This research was supported financially by the National Natural Science Foundation of China (92062218, 41822304).

Manuscript received Jan. 17, 2022
accepted Mar. 11, 2022
associate EIC: FANG Xiang
edited by Susan TURNER and FANG Xiang

References

Badullovich, N., Moynier, F., Creech, J., Teng, F.Z., and Sossi, P.A., 2017. Tin isotopic fractionation during igneous differentiation and Earth's mantle composition. Geochemical Perspectives Letters, 5: 24−28.

Bailey, J.C., 1977. Fluorine in granitic rocks and melts: A review. Chemical Geology, 19: 1−42.

Bajnóczi, É.G., Czeglédi, E., Kuzmann, E., Homonnay, Z., Bálint, S., and Dombi, G., 2014. Speciation and structure of tin (II) in hyper-alkaline aqueous solution. Dalton Transactions, 43: 17971−17979.

Barsukov, V.L., and Sushchevskaya, T.M., 1973. Evolution of composition of hydrothermal solutions in the formation of tin-ore deposits. Geochemistry International, 10: 363−375.

Becke, A.D., 1993a. Density-functional thermochemistry. III. The role of exact exchange. The Journal of Chemical Physics, 98: 5648−5652.

Becke, A.D., 1993b. A new mixing of Hartree–Fock and local density–functional theories. The Journal of Chemical Physics, 98(2): 1372−1377.

Bigeleisen, J., and Mayer, M.G., 1947. Calculation of equilibrium constants for isotopic exchange reactions. The Journal of Chemical Physics, 15(5): 261−267.

Blanchard, M., Balan, E., and Schauble, E.A., 2017. Equilibrium fractionation of non-traditional isotopes: A molecular modeling perspective. Reviews in Mineralogy and Geochemistry, 82(1): 27−63.

Bond, A.M., and Taylor, R.J., 1970. Polarographic studies of the fluoride complexes of tin (II) in neutral and acidic media. Journal of Electroanalytical Chemistry and Interfacial Electrochemistry, 28(1): 207−215.

Brugger, J., Liu, W., Etschmann, B., Mei, Y., Sherman, D.M., and Testemale, D., 2016. A review of the coordination chemistry of hydrothermal systems, or do coordination changes make ore deposits? Chemical Geology, 447: 219−253.

Chacko, T., Cole, D.R., and Horita, J., 2001. Equilibrium oxygen, hydrogen and carbon isotope fractionation factors applicable to geologic systems. Reviews in Mineralogy and Geochemistry, 43(1): 1−81.

Chen, X., and Grandbois, M., 2013. In situ Raman spectroscopic observation of sequential hydrolysis of stannous chloride to abhurite, hydroromarchite, and romarchite. Journal of Raman

Spectroscopy, 44(3): 501−506.
Cigala, R.M., Crea, F., De, Stefano, C., Lando, G., Milea, D., and Sammartano, S., 2012. The inorganic speciation of tin (II) in aqueous solution. Geochimica et Cosmochimica Acta, 87: 1−20.
Collins, P.L.F., 1981. The geology and genesis of the Cleveland tin deposit, western Tasmania: Fluid inclusion and stable isotope studies. Economic Geology, 76(2): 365−392.
Creech, J.B., Moynier, F., and Badullovich, N., 2017. Tin stable isotope analysis of geological materials by double-spike MC−ICP−MS. Chemical Geology, 457: 61−67.
Dauphas, N., and Schauble, E.A., 2016. Mass fractionation laws, mass-independent effects, and isotopic anomalies. Annual Review of Earth and Planetary Sciences, 44: 709−783.
Djurdjevic, P., Jelic, R., Djokic, D., and Veselinovic, D., 1995. Hydrolysis of tin (II) ion in sodium chloride medium. Journal−Serbian Chemical Society, 60: 785−785.
Dokic, D., Zmbova, B., Veselinovic, D., and Durevic, P., 1991. Investigation on tin (II)−hippuric acid system in perchlorate medium. Journal−Serbian Chemical Society, 56: 661−669.
Duc-Tin, Q., Audétat, A., and Keppler, H., 2007. Solubility of tin in (Cl, F)-bearing aqueous fluids at 700°C, 140 MPa: A LA−ICP−MS study on synthetic fluid inclusions. Geochimica et Cosmochimica Acta, 71: 3323−3335.
Eadington, P.J., 1983. A fluid inclusion investigation of ore formation in a tin-mineralized granite, New England, New South Wales. Economic Geology, 78(6): 1204−1221.
Edwards, R., Gillard, R.D., and Williams, P.A., 1996. The stabilities of secondary tin minerals. The hydrolysis of tin (II) sulphate and of $Sn_3O(OH)_2SO_4$. Mineralogical Magazine, 60: 427−432.
Gao, C., and Liu, Y., 2021. First-principles calculations of equilibrium bromine isotope fractionations. Geochimica et Cosmochimica Acta, 297: 65−81.
Guo, J., Zhang, R., Sun, W., Ling, M., Hu, Y., Wu, K., Luo, M., and Zhang, L., 2018. Genesis of tin-dominant polymetallic deposits in the Dachang district, South China: Insights from cassiterite U-Pb ages and trace element compositions. Ore Geology Reviews, 95: 863−879.
Halley, S.W., and Walshe, J.L., 1995. A reexamination of the Mount Bischoff cassiterite sulfide skarn, western Tasmania. Economic Geology, 90(6): 1676−1693.
Heinrich, C.A., 1990. The chemistry of hydrothermal tin (−tungsten) ore deposition. Economic Geology, 85(3): 457−481.
Helgeson, H.C., 1969. Thermodynamics of hydrothermal systems at elevated temperatures and pressures. American Journal of Science, 267(7): 729−804.
Huang, F., Chen, L., Wu, Z., and Wang, W., 2013. First-principles calculations of equilibrium Mg isotope fractionations between garnet, clinopyroxene, orthopyroxene, and olivine: Implications for Mg isotope thermometry. Earth and Planetary Science Letters, 367: 61−70.
Huang, F., Wu, Z., Huang, S., and Wu, F., 2014. First-principles calculations of equilibrium silicon isotope fractionation among mantle minerals. Geochimica et Cosmochimica Acta, 140: 509−520.
Huang, F., Zhou, C., Wang, W., Kang, J., and Wu, Z., 2019. First -principles calculations of equilibrium Ca isotope fractionation: Implications for oldhamite formation and evolution of lunar magma ocean. Earth and Planetary Science Letters, 510: 153−160.
Jackson, K.J., and Helgeson, H.C., 1985. Chemical and thermodynamic constraints on the hydrothermal transport and deposition of tin: I. Calculation of the solubility of cassiterite at high pressures and temperatures. Geochimica et Cosmochimica Acta, 49(1): 1−22.
Lee, C., Yang, W., and Parr, R.G., 1988. Development of the Colle−Salvetti correlation−energy formula into a functional of the electron density. Physical review B, 37(2): 785.
Lehmann, B., 1990. Large-scale tin depletion in the Tanjungpandan tin granite, Belitung Island, Indonesia. Economic Geology, 85(1): 99−111.
Lehmann, B. 2021. Formation of tin ore deposits: A reassessment. Lithos, 402: 105756.
Li, X., and Liu, Y., 2011. Equilibrium Se isotope fractionation parameters: A first-principles study. Earth and Planetary Science Letters, 304(1−2): 113−120.
Li, X., Zhao, H., Tang, M., and Liu, Y., 2009. Theoretical prediction for several important equilibrium Ge isotope fractionation factors and geological implications. Earth and Planetary Science Letters, 287(1−2): 1−11.
Liu, Q., Tossell, J. A., and Liu, Y., 2010. On the proper use of the Bigeleisen−Mayer equation and corrections to it in the calculation of isotopic fractionation equilibrium constants. Geochimica et Cosmochimica Acta, 74(24): 6965–6983.
Liu, P., Mao, J., Lehmann, B., Weyer, S., Horn, I., Mathur, R Zhou, Z., 2021. Tin isotopes via fs−LA−MC−ICP−MS analysis record complex fluid evolution in single cassiterite crystals. American Mineralogist: Journal of Earth and Planetary Materials, 106(12): 1980−1986.
Liu, Y., and Tossell, J.A., 2005. Ab initio molecular orbital calculations for boron isotope fractionations on boric acids and borates. Geochimica et Cosmochimica Acta, 69(16): 3995−4006.
Liu, Y., Li, J., and Chou, I.M., 2020. Cassiterite crystallization experiments in alkali carbonate aqueous solutions using a hydrothermal diamond−anvil cell. American Mineralogist: Journal of Earth and Planetary Materials, 105(5): 664−673.
Mao, J.W., Yuan, S.D., Xie, G.Q., Song, S.W., Zhou, Q., Gao, Y.B., Liu, X., Fu X.F., Cao, J., Zeng Z. L., Li T.G., and Fan, X.Y., 2019. New advances on metallogenic studies and exploration on critical minerals of China in 21st century. Mineral Deposits, 38: 935−969 (in Chinese with English abstract).
Mao, J.W, Zheng, W., Xie, G.Q, Lehmann, B., and Goldfarb, R., 2021. Recognition of a Middle–Late Jurassic arc-related porphyry copper belt along the southeast China coast: Geological characteristics and metallogenic implications. Geology, 49(5): 592−596.
Mason, A.H., Powell, W.G., Bankoff, H.A., Mathur, R., Bulatović, A., Filipović, V., and Ruiz, J., 2016. Tin isotope characterization of bronze artifacts of the central Balkans. Journal of Archaeological Science, 69: 110−117.
Mathur, R., Powell, W., Mason, A., Godfrey, L., Yao, J., and Baker, M.E., 2017. Preparation and measurement of cassiterite for Sn isotope analysis. Geostandards and Geoanalytical Research, 41(4): 701−707.
Mohamed, M.A.M., 2013. Evolution of mineralizing fluids of cassiterite–wolframite and fluorite deposits from Mueilha tin mine area, Eastern Desert of Egypt, evidence from fluid inclusion. Arabian Journal of Geosciences, 6(3): 775−782.
Müller, B., and Seward, T.M., 2001. Spectrophotometric determination of the stability of tin (II) chloride complexes in aqueous solution up to 300°C. Geochimica et Cosmochimica Acta, 65(22): 4187−4199.
Pettine, M., Millero, F.J., and Macchi, G., 1981. Hydrolysis of tin (II) in aqueous solutions. Analytical Chemistry, 53(7): 1039−1043.
Roskosz, M., Amet, Q., Fitoussi, C., Dauphas, N., Bourdon, B., Tissandier, L., and Alp, E.E., 2020. Redox and structural controls on tin isotopic fractionations among magmas. Geochimica et Cosmochimica Acta, 268: 42−55.
Schauble, E.A., 2004. Applying stable isotope fractionation theory to new systems. Reviews in mineralogy and geochemistry, 55(1): 65−111.
Schauble, E.A., Rossman, G.R., and Taylor, Jr.H.P., 2003. Theoretical estimates of equilibrium chlorine−isotope fractionations. Geochimica et Cosmochimica Acta, 67(17): 3267−3281.
Schmidt, C., 2018. Formation of hydrothermal tin deposits: Raman spectroscopic evidence for an important role of aqueous Sn (IV) species. Geochimica et Cosmochimica Acta, 220: 499−511.
Séby, F., Potin-Gautier, M., Giffaut, E., and Donard, O.F.X., 2001. A critical review of thermodynamic data for inorganic tin species. Geochimica et Cosmochimica Acta, 65(18): 3041−3053.
She, J.X., Wang, T., Liang, H., Muhtar, M.N., Li,W., and Liu, X., 2020. Sn isotope fractionation during volatilization of Sn

(IV) chloride: Laboratory experiments and quantum mechanical calculations. Geochimica et Cosmochimica Acta, 269: 184−202.

Sherman, D. M., Ragnarsdottir, K.V., Oelkers, E.H., and Collins, C.R., 2000. Speciation of tin (Sn^{2+} and Sn^{4+}) in aqueous Cl solutions from 25° C to 350° C: An in-situ EXAFS study. Chemical Geology, 167(1−2): 169−176.

Tossell, J. A., 2005. Calculating the partitioning of the isotopes of Mo between oxidic and sulfidic species in aqueous solution. Geochimica et Cosmochimica Acta, 69(12): 2981−2993.

Uchida, E., Sakamori, T., and Matsunaga, J., 2002. Aqueous speciation of lead and tin chlorides in supercritical hydrothermal solutions. Geochemical Journal, 36(1): 61−72.

Urey, H.C., 1947. The thermodynamic properties of isotopic substances. Journal of the Chemical Society (Resumed), 562−581.

Wang, D., Mathur, R., Powell, W., Godfrey, L., and Zheng, Y., 2019. Experimental evidence for fractionation of tin chlorides by redox and vapor mechanisms. Geochimica et Cosmochimica Acta, 250: 209−218.

Wang, R.C., Yu, A.P., Chen, J., Xie, L., Lu, J.J., and Zhu, J.C., 2012. Cassiterite exsolution with ilmenite lamellae in magnetite from the Huashan metaluminous tin granite in southern China. Mineralogy and Petrology, 105(1): 71−84.

Wang, T., She, J.X., Yin, K., Wang, K., Zhang, Y., Lu, X., and Li, W., 2021. Sn(II) chloride speciation and equilibrium Sn isotope fractionation under hydrothermal conditions: A first principles study. Geochimica et Cosmochimica Acta, 300: 25−43.

Wang, X., Amet, Q., Fitoussi, C., and Bourdon, B., 2018. Tin isotope fractionation during magmatic processes and the isotope composition of the bulk silicate Earth. Geochimica et Cosmochimica Acta, 228: 320−335.

White, W.H., Bookstrom, A.A., Kamilli, R.J., Ganster, M.W., Smith, R., Ranta, D.E., and Steininger, R.C., 1981. Character and origin of Climax-type molybdenum deposits. Economic Geology, 75: 270−316.

Yao, J., Mathur, R., Powell, W., Lehmann, B., Tornos, F., Wilson, M., and Ruiz, J., 2018. Sn-isotope fractionation as a record of hydrothermal redox reactions. American Mineralogist, 103(10): 1591−1598.

Young, E.D., Tonui, E., Manning, C.E., Schauble, E., and Macris, C.A., 2009. Spinel–olivine magnesium isotope thermometry in the mantle and implications for the Mg isotopic composition of Earth. Earth and Planetary Science Letters, 288: 524–533.

Yuan, S., Williams-Jones, A.E., Romer, R.L., Zhao, P., and Mao, J., 2019. Protolith-related thermal controls on the decoupling of Sn and W in Sn−W metallogenic provinces: Insights from the Nanling region, China. Economic Geology, 114(5): 1005−1012.

Yuan, S., Zhao, P., and Liu, M., 2020. Some problems involving in petrogenesis and metallogenesis of granite-related tin deposits. Mineral Deposits, 39(4): 607−618 (in Chinese with English abstract).

Zhu, C., and Sverjensky, D.A., 1992. F−Cl−OH partitioning between biotite and apatite. Geochimica et Cosmochimica Acta, 56(9): 3435−3467.

About the first author

SUN Mingguang, male, born in 1990 in Liaocheng, Shandong Province; Ph.D. candidate; Institute of Mineral Resources, Chinese Academy of Geological Sciences, Beijing. He is now interested in experimental and theoretical studies of the thermodynamics and molecular mechanisms of hydrothermal ore-forming systems. E-mail: 846640311@qq.com.

About the corresponding author

WANG Jiaxin, male, born in 1988 in Zhangjiakou, Hebei Province; Ph.D.; graduated from China University of Geosciences, Beijing; assistant researcher, Institute of Mineral Resources, Chinese Academy of Geological Sciences. He is now interested in experimental and theoretical studies of the thermodynamics and molecular mechanisms of hydrothermal ore-forming systems. E-mail: jiaxin.wang@cags.ac.cn.